

Electronic properties of graphene with a topological defect

Yu.A. Sitenko^{1,2} and N.D. Vlasii^{1,2}

¹Bogolyubov Institute for Theoretical Physics,
National Academy of Sciences, 03680, Kyiv, Ukraine

²Physics Department, National Taras Shevchenko University of Kyiv,
03127, Kyiv 127, Ukraine

Various types of topological defects in graphene are considered in the framework of the continuum model for long-wavelength electronic excitations, which is based on the Dirac–Weyl equation. The condition for the electronic wave function is specified, and we show that a topological defect can be presented as a pseudomagnetic vortex at the apex of a graphitic nanocone; the flux of the vortex is related to the deficit angle of the cone. The cases of all possible types of pentagonal defects, as well as several types of heptagonal defects (with the numbers of heptagons up to three, and six), are analyzed. The density of states and the ground state charge are determined.

PACS: 11.10.-z, 73.43.Cd, 73.61.Wp, 81.05.Uw

Keywords: graphitic nanocones, disclinations, vortex, Dirac–Weyl equation, self-adjoint extension, density of states

1 Introduction

A synthesis of strictly twodimensional crystals composed of carbon atoms (graphene) [1] is promising a wealth of new phenomena and possible applications in technology and industry [2]. The observation of anomalous transport properties, and, most exciting, the recent discovery of substantial field effect and magnetism at room temperature allows one to envisage graphene as a reasonable replacement of nanotubes in electronic applications, see, e.g., Refs. [3, 4, 5].

By symmetry, the valence and conduction bands in graphene touch at the corners of the hexagonal Brillouin zone. In the vicinity of these points, the dispersion relation is isotropic and linear, and the density of states at the Fermi level

is strictly zero, rising linearly in energy. An effective long-wavelength description of these electronic states can be written in terms of a continuum model which is based on the Dirac–Weyl equation for massless electrons in 2+1-dimensional space-time [6, 7].

Lowdimensional quantum systems of Dirac fermions can possess rather unusual properties and, since the discovery of the effect of charge fractionalization [8], are generating current interest. Planar Dirac fermions in the background of the Abrikosov–Nielsen–Olesen vortex [9, 10] were studied in Ref. [11], and, recently, the results of this work have been used to consider the influence of the Kekulé distortion in the honeycomb lattice on the electronic properties of graphene [12, 13]. The present paper deals with yet another aspect, and our purpose is to elucidate the role of topological defects in the graphene lattice.

Topological defects appear as a result of removing (inserting) one or several carbon atoms from (into) the honeycomb lattice without affecting the threefold coordination of other atoms; appropriately, the lattice surface is warped owing to positive (negative) curvature induced at the location of a defect. Assuming that the size of a defect is small as compared to the whole size of the graphene sample, our interest will be in the study of the influence of such a defect on the electronic properties of graphene. The consideration is based on the continuum model for long-wavelength electronic excitations, and various types of defects are characterized by just the number of carbon atoms removed or inserted; actually, the size of a defect is neglected. The graphene sheet with a defect takes shape of a cone with the value of the apex angle related to the number of removed atoms. When a defect is encircled, then sublattices, as well as inequivalent Fermi points, are entwined or left untwined, depending on the type of a defect. This imposes a condition on the electronic wave function on the graphene sheet: a phase is acquired under a rotation around a defect. If the phase commutes with the hamiltonian, then it can be eliminated by a singular gauge transformation which, on the other hand, introduces a fictitious point vortex that may be denoted in the following as a pseudomagnetic one. The flux of the pseudomagnetic vortex is related to the deficit (profit) angle of the conical surface, i.e. to the number of removed (inserted) atoms. For certain types of defects the vortex flux takes fractional values in the units of 2π .

A general theory of planar relativistic fermionic systems in the background of a point magnetic vortex with arbitrary flux was proposed in Refs. [14, 15]; in particular, the case of massless fermions was considered in Refs. [16, 17]. If the vortex flux is fractional in the units of the London flux, then an essentially irregular mode appears among the eigenmodes of the one-particle hamiltonian, and this in its turn gives rise to the appearance of an additional parameter – the self-adjoint extension parameter which specifies the boundary condition at the vortex point [18]. The theory allows us to predict the density of states (not

local but total) [19] and the ground state quantum numbers, as well as their local densities [15, 16, 17]. The aim of the present paper is to apply this theory to graphene with a topological defect. The previous attempts to consider the electronic properties of graphene with topological defects in the framework of the continuum model approach [20, 21, 22] have led to contradictory and, therefore, unconvincing results. In our opinion, this is due to the two circumstances: an inadequate choice of the condition for the electronic wave function in the case of the entwinement of sublattices and an inappropriate treatment of irregular eigenmodes of the one-particle hamiltonian. These deficiencies will be remedied in the present study.

In the next section we review the derivation of the continuum model for planar graphene in order to specify the notations used. In Section 3 we introduce topological defects in graphene in the framework of the continuum model, derive the condition for the electronic wave function in the case of an arbitrary defect, and demonstrate that the defect can be presented as a pseudomagnetic vortex at the apex of a graphitic nanocone. In Section 4 we consider the solution of the Dirac–Weyl equation for electronic excitations on a graphene sheet with a topological defect and find the density of states and the ground state charge. The results are discussed in Section 5. In Appendix A we show that the case of the three-pentagon defect coincides actually with that of the absence of defects. In Appendix B the method of a self-adjoint extension is applied to derive the condition for the irregular solution to the Dirac–Weyl equation.

2 Continuum model for long-wavelength electronic excitations

Carbon atoms in graphene form a honeycomb lattice. The Bravais lattice is triangular, and the primitive cell is rhombic and contains two carbon atoms. If one atom is placed at the origin of the primitive cell, another one is displaced at $\mathbf{d} = (-d, 0)$, where d is the lattice spacing. Thus, the honeycomb lattice is composed of two triangular sublattices: sublattice Λ_A (black points) is generated by vectors $\mathbf{r}_i = n_i \mathbf{c}_1 + m_i \mathbf{c}_2$, and sublattice Λ_B (blank points) is generated by vectors $\mathbf{r}_i = n_i \mathbf{c}_1 + m_i \mathbf{c}_2 + \mathbf{d}$, where $\mathbf{c}_1 = \left(\frac{3}{2}d, \frac{\sqrt{3}}{2}d\right)$ and $\mathbf{c}_2 = \left(\frac{3}{2}d, -\frac{\sqrt{3}}{2}d\right)$ are the basis vectors of the primitive cell (see Fig.1a), and $n_i, m_i \in \mathbb{Z}$ (\mathbb{Z} is the set of integer numbers).

Each carbon atom in graphene has four valence electrons. As a result of hybridization, three of them build σ -orbitals along the lattice links providing for their rigidity, while the fourth one makes π -orbital which is orthogonal to the lattice plane and is responsible for the conductive properties of graphene.

Retaining only nearest neighbour interactions in the tight-binding approximation, quantum-mechanical hopping of an electron on a planar honeycomb lattice is described with the use of hamiltonian

$$\mathcal{H} = -t \sum_{i \in \Lambda_A} \sum_{j=1}^3 a^\dagger(\mathbf{r}_i) b(\mathbf{r}_i + \mathbf{u}_j) - t \sum_{i \in \Lambda_B} \sum_{j=1}^3 b^\dagger(\mathbf{r}_i) a(\mathbf{r}_i + \mathbf{v}_j), \quad (1)$$

where t is the hopping amplitude, $a^\dagger(\mathbf{r}_i)$ and $a(\mathbf{r}_i)$ ($b^\dagger(\mathbf{r}_i)$ and $b(\mathbf{r}_i)$) are the creation and destruction operators acting on sublattice Λ_A (Λ_B), which obey anticommutation relations

$$[a(\mathbf{r}_i), a^\dagger(\mathbf{r}_{i'})]_+ = [b(\mathbf{r}_i), b^\dagger(\mathbf{r}_{i'})]_+ = \delta_{ii'},$$

\mathbf{u}_j (\mathbf{v}_j) are the triad of vectors which are directed to the nearest neighbours of an atom belonging to sublattice Λ_A (Λ_B), see Fig.1b,

$$\begin{aligned} \mathbf{u}_1 &= (-d, 0), & \mathbf{u}_2 &= \left(\frac{1}{2}d, \frac{\sqrt{3}}{2}d\right), & \mathbf{u}_3 &= \left(\frac{1}{2}d, -\frac{\sqrt{3}}{2}d\right), \\ \mathbf{v}_1 &= (d, 0), & \mathbf{v}_2 &= \left(-\frac{1}{2}d, -\frac{\sqrt{3}}{2}d\right), & \mathbf{v}_3 &= \left(-\frac{1}{2}d, \frac{\sqrt{3}}{2}d\right). \end{aligned} \quad (2)$$

Using the Fourier transforms of the sublattice operators,

$$a(\mathbf{r}_i) = \int_{\Gamma} \frac{d^2k}{(2\pi)^2} e^{i\mathbf{k}\mathbf{r}_i} \tilde{a}(\mathbf{k}), \quad b(\mathbf{r}_i) = \int_{\Gamma} \frac{d^2k}{(2\pi)^2} e^{i\mathbf{k}\mathbf{r}_i} \tilde{b}(\mathbf{k}),$$

where Γ is the first Brillouin zone, hamiltonian (1) is presented as

$$\mathcal{H} = \int_{\Gamma} \frac{d^2k}{(2\pi)^2} \tilde{\psi}^\dagger(\mathbf{k}) \tilde{H} \tilde{\psi}(\mathbf{k}), \quad (3)$$

where

$$\tilde{\psi}(\mathbf{k}) = \left(\tilde{a}(\mathbf{k}), \tilde{b}(\mathbf{k}) \right)^T, \quad \tilde{\psi}^\dagger(\mathbf{k}) = \left(\tilde{a}^\dagger(\mathbf{k}), \tilde{b}^\dagger(\mathbf{k}) \right),$$

and

$$\tilde{H} = \begin{pmatrix} 0 & -t \sum_{j=1}^3 e^{i\mathbf{k}\mathbf{u}_j} \\ -t \sum_{j=1}^3 e^{i\mathbf{k}\mathbf{v}_j} & 0 \end{pmatrix}. \quad (4)$$

Solving the eigenvalue problem, $\tilde{H} \tilde{\psi}(\mathbf{k}) = E \tilde{\psi}(\mathbf{k})$, one gets

$$\begin{aligned} E &= \pm t \sqrt{\sum_{j=1}^3 e^{i\mathbf{k}\mathbf{u}_j} \sum_{j'=1}^3 e^{i\mathbf{k}\mathbf{v}_{j'}}} = \\ &= \pm t \sqrt{1 + 4 \cos\left(\frac{\sqrt{3}}{2}k_y d\right) \left[\cos\left(\frac{3}{2}k_x d\right) + \cos\left(\frac{\sqrt{3}}{2}k_y d\right) \right]}. \end{aligned} \quad (5)$$

As follows from Eq.(5), the one-particle energy spectrum consists of two surfaces ($E > 0$ and $E < 0$) which intersect ($E = 0$) at six conical points that are located at

$$\begin{aligned} k_x &= 0, & k_y &= \pm 4\pi(3\sqrt{3}d)^{-1}, \\ k_x &= \pm 2\pi(3d)^{-1}, & k_y &= \pm 2\pi(3\sqrt{3})d^{-1}. \end{aligned} \quad (6)$$

With one electron per site, the negative-energy states (valence band) are filled and the positive-energy states (conduction band) are empty, so the band structure is at half-filling with the Fermi level $E = 0$ corresponding to six isolated points given in Eq.(6). The first Brillouin zone is a hexagon with corners identified with these Fermi points; among six of them, only two ones which can be taken as oppositely located are inequivalent, see Fig.2.

Actually, \tilde{H} (4) has the meaning of the one-particle hamiltonian in the momentum representation. The low-energy excitations can be studied by taking the continuum limit ($d \rightarrow 0$) at any of two inequivalent Fermi points. Choosing the pair of inequivalent points as $\mathbf{K}_{\pm} = (0, \pm 4\pi(3\sqrt{3}d)^{-1})$ and keeping terms of order $\mathbf{k} - \mathbf{K}_{\pm}$, one gets :

$$\tilde{H}_{\pm} = \lim_{d \rightarrow 0} d^{-1} \tilde{H}|_{\mathbf{k}=\mathbf{K}_{\pm}+\boldsymbol{\kappa}} = \frac{3}{2}t \begin{pmatrix} 0 & i\kappa_x \pm \kappa_y \\ -i\kappa_x \pm \kappa_y & 0 \end{pmatrix} = \hbar v(-\sigma^2 \kappa_x \pm \sigma^1 \kappa_y), \quad (7)$$

where $v = \frac{3}{2}t\hbar^{-1}$ is the Fermi velocity, and σ^1 and σ^2 are the off-diagonal Pauli matrices. Combining the contributions from \mathbf{K}_+ and \mathbf{K}_- , one gets

$$\begin{pmatrix} \tilde{H}_+ & 0 \\ 0 & \tilde{H}_- \end{pmatrix} = \hbar v (\alpha^1 \kappa_x + \alpha^2 \kappa_y), \quad (8)$$

where

$$\alpha^1 = - \begin{pmatrix} \sigma^2 & 0 \\ 0 & \sigma^2 \end{pmatrix}, \quad \alpha^2 = \begin{pmatrix} \sigma^1 & 0 \\ 0 & -\sigma^1 \end{pmatrix}. \quad (9)$$

Making the Fourier transformation of Eq.(8), one gets the long-wavelength approximation for the one-particle hamiltonian operator

$$H = -i\hbar v(\alpha^1 \partial_x + \alpha^2 \partial_y), \quad (10)$$

which acts on four-component wave functions of the form

$$\psi = (\psi_{A+}, \psi_{B+}, \psi_{A-}, \psi_{B-})^T, \quad (11)$$

where subscripts A and B correspond to two sublattices and subscripts $+$ and $-$ correspond to two inequivalent Fermi points. Thus, an effective long-wavelength description of charge carriers in graphene is written in terms of a continuum

model which is based on the Dirac–Weyl equation for massless electrons in 2 + 1-dimensional space-time, with the role of speed of light c played by Fermi velocity $v \approx c/300$ [6, 7], see also Ref. [23].

In order to complete the Clifford algebra of anticommuting 4×4 matrices, one has to define γ^0 , γ^3 , and $\gamma^5 = -i\gamma^0\gamma^1\gamma^2\gamma^3$ (where $\boldsymbol{\gamma} = \gamma^0\boldsymbol{\alpha}$). It should be noted that hamiltonian (10) commutes with generators T_k ($k = 1, 2, 3$) of the $SU(2)$ -symmetry transformations, $[T_k, T_l] = i\varepsilon_{klm}T_m$, where

$$T_1 = \frac{i}{2}\gamma^3, \quad T_2 = \frac{1}{2}\gamma^5, \quad T_3 = \frac{1}{2}\gamma^3\gamma^5, \quad (12)$$

and there is an arbitrariness in the choice of the representation of the Clifford algebra, which is due to a possibility of diagonalizing anyone of T_k . A representation with diagonal γ^0 , in view of the block-diagonal form of α^1 and α^2 , see Eq.(9), corresponds to the choice of diagonal T_3 and may be denoted as the standard planar representation:

$$\begin{aligned} \gamma^0 &= \begin{pmatrix} \sigma^3 & 0 \\ 0 & \sigma^3 \end{pmatrix}, & \gamma^1 &= i \begin{pmatrix} \sigma^1 & 0 \\ 0 & \sigma^1 \end{pmatrix}, & \gamma^2 &= i \begin{pmatrix} \sigma^2 & 0 \\ 0 & -\sigma^2 \end{pmatrix}, \\ \gamma^3 &= i \begin{pmatrix} 0 & \sigma^2 \\ \sigma^2 & 0 \end{pmatrix}, & \gamma^5 &= i \begin{pmatrix} 0 & -\sigma^2 \\ \sigma^2 & 0 \end{pmatrix}. \end{aligned} \quad (13)$$

Choosing T_2 to be diagonal, one gets the chiral planar representation:

$$\begin{aligned} \gamma^0 &= \begin{pmatrix} 0 & \sigma^1 \\ \sigma^1 & 0 \end{pmatrix}, & \gamma^1 &= -i \begin{pmatrix} 0 & \sigma^3 \\ \sigma^3 & 0 \end{pmatrix}, & \gamma^2 &= \begin{pmatrix} 0 & -1 \\ 1 & 0 \end{pmatrix}, \\ \gamma^3 &= -i \begin{pmatrix} 0 & \sigma^2 \\ \sigma^2 & 0 \end{pmatrix}, & \gamma^5 &= \begin{pmatrix} -1 & 0 \\ 0 & 1 \end{pmatrix}. \end{aligned} \quad (14)$$

A rotation by angle ϑ in the plane of a graphene sheet is implemented by operator $\exp(i\vartheta\Sigma)$, where

$$\Sigma = \frac{1}{2i}\alpha^1\alpha^2 = \frac{1}{2} \begin{pmatrix} \sigma^3 & 0 \\ 0 & -\sigma^3 \end{pmatrix} \quad (15)$$

is the pseudospin playing here the role of the operator of spin component which is orthogonal to the plane. The honeycomb lattice is invariant under the rotation by 2π ,

$$\exp(i2\pi\Sigma)\psi = -\psi, \quad (16)$$

but is not invariant under the rotation by π ,

$$\exp(i\pi\Sigma)\psi = 2i\Sigma\psi,$$

i.e. under $x \rightarrow -x$ and $y \rightarrow -y$. However, if the latter rotation is supplemented by simultaneous exchange of sublattices, as well as Fermi points, then this combined transformation,

$$R \exp(i\pi\Sigma)\psi = i(\psi_{B-}, \psi_{A-}, \psi_{B+}, \psi_{A+})^T, \quad (17)$$

is a symmetry one and can be regarded as the parity transformation for graphene. Note that transformation (17) is implemented by $i\alpha^3 \equiv i\gamma^0\gamma^3$ in the standard planar representation, see Eq.(13), or by $i\gamma^0$ in the chiral planar representation, see Eq.(14). The explicit form of R is extracted from Eq.(17):

$$R = i \begin{pmatrix} 0 & \sigma^2 \\ -\sigma^2 & 0 \end{pmatrix}, \quad (18)$$

and it is given by $-\gamma^5$ in representation (13) or by $-\gamma^3\gamma^5$ in representation (14). Note that R is commuting with Σ (15) and H (10).

3 Topological defects

Topological defects in graphene are disclinations in the honeycomb lattice, resulting from the substitution of a hexagon by, say, a pentagon or a heptagon; such a disclination warps the graphene sheet. More generally, a hexagon is substituted by a polygon with $6 - N_d$ sides, where N_d is an integer which is smaller than 6. Polygons with $N_d > 0$ ($N_d < 0$) induce locally positive (negative) curvature, whereas the graphene sheet is flat away from the defect, as is the conical surface away from the apex. In the case of nanocones with $N_d > 0$, the value of N_d is related to apex angle δ ,

$$\sin \frac{\delta}{2} = 1 - \frac{N_d}{6}, \quad (19)$$

and N_d counts the number of sectors of the value of $\pi/3$ removed from the graphene sheet, see Fig.3a. If $N_d < 0$, then $-N_d$ counts the number of such sectors inserted into the graphene sheet. Certainly, polygonal defects with $N_d > 1$ and $N_d < -1$ are mathematical abstractions, as are cones with a pointlike apex. In reality, the defects are smoothed, and $N_d > 0$ counts the number of the pentagonal defects which are tightly clustered producing a conical shape; such nanocones were observed experimentally [24]. Theory predicts also an infinite series of the saddle-like nanocones with $-N_d$ counting the number of the heptagonal defects clustered in their central regions. However, as it was shown by using molecular-dynamics simulations [25], in the case of $N_d \leq -4$, a surface with a polygonal defect is more stable than a similarly shaped surface containing a multiple number of heptagons; a screw dislocation can be presented as the $N_d \rightarrow -\infty$ limit of a $6 - N_d$ -gonal defect.

The twodimensional Dirac–Weyl hamiltonian on a curved surface with the squared length element $ds^2 = g_{jj'}(\mathbf{r})dr^j r^{j'}$ takes form (see, e.g., Ref.[26])

$$H = -i\hbar v \tilde{\alpha}^j(\mathbf{r}) \left[\partial_j + \frac{i}{2} \omega_j(\mathbf{r}) \right], \quad (20)$$

where

$$\left[\tilde{\alpha}^j(\mathbf{r}), \tilde{\alpha}^{j'}(\mathbf{r}) \right]_+ = 2g^{jj'}(\mathbf{r})I \quad (21)$$

and

$$\begin{aligned} \omega_j(\mathbf{r}) &= -\frac{i}{2} \tilde{\alpha}^k(\mathbf{r}) \left[\partial_j \tilde{\alpha}_k(\mathbf{r}) - \Gamma_{jk}^l(\mathbf{r}) \tilde{\alpha}_l(\mathbf{r}) \right], \\ \Gamma_{jk}^l(\mathbf{r}) &= \frac{1}{2} g^{ln}(\mathbf{r}) \left[\partial_j g_{nk}(\mathbf{r}) + \partial_k g_{nj}(\mathbf{r}) - \partial_n g_{jk}(\mathbf{r}) \right]. \end{aligned} \quad (22)$$

In the case of a conical surface with a pointlike apex, one has

$$g_{rr} = 1, \quad g_{\varphi\varphi} = (1 - \eta)^2 r^2, \quad (23)$$

where r and φ are polar coordinates centred at the apex, and $-\infty < \eta < 1$. The intrinsic curvature of a cone vanishes at $\mathbf{r} \neq 0$ and possesses a $\delta^2(\mathbf{r})$ -singularity at its apex ($\mathbf{r} = 0$); parameter η enters the coefficient before this singularity term. Introducing $\varphi' = (1 - \eta)\varphi$, one gets the metric in the (r, φ') coordinates, which is identical to that of a plane, but with φ' in the range $0 < \varphi' < 2\pi(1 - \eta)$. Thus, quantity $2\pi\eta$ for $0 < \eta < 1$ is the deficit angle measuring the magnitude of the removed sector, and quantity $-2\pi\eta$ for $-\infty < \eta < 0$ is the proficit angle measuring the magnitude of the inserted sector. In the case of graphitic nanocones, parameter η takes discrete values:

$$\eta = N_d/6. \quad (24)$$

Using Eqs.(21) and (23), one gets

$$\tilde{\alpha}^r = \alpha^1, \quad \tilde{\alpha}^\varphi = (1 - \eta)^{-1} r^{-1} \alpha^2. \quad (25)$$

It is straightforward to calculate the nonvanishing Christoffel symbols

$$\Gamma_{r\varphi}^\varphi = \Gamma_{\varphi r}^\varphi = r^{-1}, \quad \Gamma_{\varphi\varphi}^r = -(1 - \eta)^2 r,$$

and get the spin connection

$$\omega_r = 0, \quad \omega_\varphi = -2(1 - \eta)\Sigma.$$

Thus, hamiltonian (20) on a conical surface takes form

$$H = -i\hbar v \left\{ \alpha^1 \partial_r + \alpha^2 r^{-1} \left[(1 - \eta)^{-1} \partial_\varphi - i\Sigma \right] \right\}. \quad (26)$$

In the case of the planar graphene sheet ($\eta = 0$), wave function (11) satisfies antiperiodicity condition, see Eq.(16),

$$\psi(r, \varphi + 2\pi) = -\psi(r, \varphi), \quad (27)$$

i.e. the wave function is a section of a bundle with spin connection -2Σ .

Let us consider a graphene sheet with a pentagonal disclination ($N_d = 1$). When circling once this defect, the two sublattices in the honeycomb structure are exchanged (see Fig.3b), the two inequivalent Fermi points are exchanged as well. Circling twice this defect is analogous to circling once a hexagon in the honeycomb lattice without defects. The situation resembles that of a Möbius strip, where a double full turn is needed to arrive at the same point. Thus, in the continuum model description of graphene with a pentagonal disclination, wave function (11) has to obey the Möbius-strip-type condition:

$$\psi(r, \varphi + 2\pi) = iR\psi(r, \varphi), \quad (28)$$

where R is given by Eq.(18), and, consequently,

$$\psi(r, \varphi + 4\pi) = -\psi(r, \varphi), \quad (29)$$

since $R^2 = I$. Note that the sign in the right hand side of Eq.(28) is chosen by convention.

In a similar way, one can show that the wave function on a graphene sheet with a heptagonal disclination ($N_d = -1$) obeys the Möbius-strip-type condition as well. Moreover, it can be noted that sublattices (and Fermi points) are entwined in the case of odd N_d and are left untwined in the case of even N_d . Thus, the condition for the wave function on a graphene sheet with an arbitrary disclination takes form

$$\psi(r, \varphi + 2\pi) = -\exp\left(-i\frac{\pi}{2}N_d R\right)\psi(r, \varphi), \quad (30)$$

where the choice of sign in the exponential function agrees with the sign choice in Eq.(28). Our results remain unchanged if the opposite sign in Eq.(28) and, correspondingly, in the exponential function in Eq.(30) is chosen.

By performing singular gauge transformation

$$\psi' = e^{i\Omega}\psi, \quad \Omega = \varphi\frac{N_d}{4}R, \quad (31)$$

one gets the wave function obeying condition

$$\psi'(r, \varphi + 2\pi) = -\psi'(r, \varphi), \quad (32)$$

in the meantime, hamiltonian (26) is transformed to

$$H' = e^{i\Omega} H e^{-i\Omega} = -i\hbar v \left\{ \alpha^1 \partial_r + \alpha^2 r^{-1} \left[(1 - \eta)^{-1} \left(\partial_\varphi - i \frac{3}{2} \eta R \right) - i \Sigma \right] \right\}, \quad (33)$$

where Eq.(24) is recalled. We conclude that a topological defect in graphene is presented by a pseudomagnetic vortex with flux $N_d \pi/2$ through the apex of a cone with deficit angle $N_d \pi/3$.

4 Ground state charge

The density of states is defined as

$$\tau(E) = \frac{1}{\pi} \text{Im Tr}(H - E - i0)^{-1}, \quad (34)$$

where Tr is the trace of an integro-differential operator in the functional space: $\text{Tr}O = \int d^2r \text{tr}\langle \mathbf{r} | O | \mathbf{r} \rangle$; tr denotes the trace over spinor indices only. Since the continuum model of graphene without topological defects corresponds to the use of the free Dirac–Weyl hamiltonian in flat twodimensional space, see Eq.(10), the density of states is immediately calculable and found to be proportional to the size of the graphene sheet

$$\tau(E) = \frac{S|E|}{\pi \hbar^2 v^2}, \quad (35)$$

where S is its area. The ground state charge of the graphene sheet,

$$Q = -\frac{e}{2} \int_{-\infty}^{\infty} dE \tau(E) \text{sgn}(E), \quad (36)$$

is evidently zero, because Eq.(35) is even in energy.

To consider the influence of topological defects in graphene on the density of states in the framework of the continuum model, we need the complete set of solutions to the Dirac–Weyl equation in this case

$$H' \psi' = E \psi', \quad (37)$$

where H' is given by Eq.(33), and ψ' is the spinor wave function obeying condition (32). In general, the contribution of a topological defect is added to Eq.(35), and, lacking the factor of area, it seems to be negligible. However, if this contribution contains a piece which is odd in energy, then the latter yields the nonzero ground state charge, see Eq.(36). In the following our interest will be in the search of

such a piece, and, as we shall see, its emergence is due to the appearance of an irregular solution to the Dirac–Weyl equation.

Let us make unitary transformation

$$\psi'' = U\psi', \quad H'' = UH'U^{-1}, \quad (38)$$

where

$$U = U^{-1} = \frac{1}{\sqrt{2}} \begin{pmatrix} I & i\sigma^2 \\ -i\sigma^2 & -I \end{pmatrix}, \quad (39)$$

then

$$URU^{-1} = \begin{pmatrix} I & 0 \\ 0 & -I \end{pmatrix} \quad (40)$$

and transformed hamiltonian H'' acquires a block-diagonal form:

$$H'' = \begin{pmatrix} H_1 & 0 \\ 0 & H_{-1} \end{pmatrix}, \quad (41)$$

where

$$H_s = \hbar v \left\{ i\sigma^2 \partial_r - \sigma^1 r^{-1} \left[(1 - \eta)^{-1} \left(is\partial_\varphi + \frac{3}{2}\eta \right) + \frac{1}{2}\sigma^3 \right] \right\}, \quad s = \pm 1. \quad (42)$$

It should be emphasized that the definite sublattice (A or B) and Fermi-point (+ or $-$) indices are assigned to the components of ψ (11), while, after performing transformations (31) and (38), one gets ψ'' with components mixing up different sublattices and Fermi points. Certainly, the calculation of functional trace in Eq.(34) does not depend on the representation used, and it is just a matter of convenience to use a representation with the block-diagonal form of hamiltonian (41).

Separating the radial and angular variables

$$\psi''(r, \varphi) = \sum_{n \in \mathbb{Z}} \langle r, \varphi | E, n \rangle, \quad (43)$$

where

$$\langle r, \varphi | E, n \rangle = \begin{pmatrix} f_{n,1}(r) e^{i(n+\frac{1}{2})\varphi} \\ g_{n,1}(r) e^{i(n+\frac{1}{2})\varphi} \\ f_{n,-1}(r) e^{i(n-\frac{1}{2})\varphi} \\ g_{n,-1}(r) e^{i(n-\frac{1}{2})\varphi} \end{pmatrix}, \quad (44)$$

one rewrites the Dirac–Weyl equation as the system of equations for the radial functions

$$\begin{pmatrix} 0 & D_{n,s}^\dagger \\ D_{n,s} & 0 \end{pmatrix} \begin{pmatrix} f_{n,s}(r) \\ g_{n,s}(r) \end{pmatrix} = E \begin{pmatrix} f_{n,s}(r) \\ g_{n,s}(r) \end{pmatrix}, \quad (45)$$

where

$$\begin{aligned} D_{n,s} &= \hbar v \left[-\partial_r + r^{-1}(1-\eta)^{-1}(sn - \eta) \right], \\ D_{n,s}^\dagger &= \hbar v \left[\partial_r + r^{-1}(1-\eta)^{-1}(sn + 1 - 2\eta) \right]. \end{aligned} \quad (46)$$

A pair of linearly independent solutions to Eq.(45) is written in terms of the cylinder functions. In the case of $\frac{1}{2} \leq \eta < 1$ ($N_d = 3, 4, 5$) the condition of regularity at the origin is equivalent to the condition of square integrability at this point, and this selects a physically reasonable solution. Thus, the situation is similar to that of $\eta = 0$ (absence of a defect), resulting in a density of states which is even in energy. In particular, it can be shown that the density of states in the case of $\eta = \frac{1}{2}$ ($N_d = 3$) is given by Eq.(35), see Appendix A.

In the case of $0 < \eta < \frac{1}{2}$ ($N_d = 1, 2$) and $-\frac{1}{2} \leq \eta < 0$ ($N_d = -1, -2, -3$) there is a mode, for which the condition of regularity at the origin is not equivalent to the condition of square integrability at this point: both linearly independent solutions for this mode are at once irregular and square integrable at the origin. To be more precise, let us define in this case

$$n_c = \frac{s}{2} [\text{sgn}(\eta) - 1], \quad (47)$$

and note that solutions to the Dirac–Weyl equation correspond to the continuous spectrum and, therefore, obey the orthonormality condition

$$\int_0^{2\pi} d\varphi \int_0^\infty dr r(1-\eta) \langle E, n | r, \varphi \rangle \langle r, \varphi | E', n' \rangle = \frac{2\delta(E - E')}{\sqrt{EE'}} \delta_{nn'}, \quad (48)$$

where a factor of 2 in the right hand side of the last relation is due to the existence of two inequivalent Fermi points. Then the complete set of solutions to Eq.(45) is chosen in the following form:

regular modes with $sn > sn_c$

$$\begin{pmatrix} f_{n,s}(r) \\ g_{n,s}(r) \end{pmatrix} = \frac{1}{2\sqrt{\pi(1-\eta)}} \begin{pmatrix} J_{l(1-\eta)^{-1}-F}(kr) \\ \text{sgn}(E) J_{l(1-\eta)^{-1}+1-F}(kr) \end{pmatrix}, \quad l = s(n - n_c), \quad (49)$$

regular modes with $sn < sn_c$

$$\begin{pmatrix} f_{n,s}(r) \\ g_{n,s}(r) \end{pmatrix} = \frac{1}{2\sqrt{\pi(1-\eta)}} \begin{pmatrix} J_{l'(1-\eta)^{-1}+F}(kr) \\ -\text{sgn}(E) J_{l'(1-\eta)^{-1}-1+F}(kr) \end{pmatrix}, \quad l' = s(n_c - n), \quad (50)$$

and an irregular mode

$$\begin{aligned} \begin{pmatrix} f_{n_c,s}(r) \\ g_{n_c,s}(r) \end{pmatrix} &= \frac{1}{2\sqrt{\pi(1-\eta)} [1 + \sin(2\nu_E) \cos(F\pi)]} \times \\ &\times \begin{pmatrix} \sin(\nu_E)J_{-F}(kr) + \cos(\nu_E)J_F(kr) \\ \text{sgn}(E) [\sin(\nu_E)J_{1-F}(kr) - \cos(\nu_E)J_{-1+F}(kr)] \end{pmatrix}, \end{aligned} \quad (51)$$

where $k = |E|(\hbar v)^{-1}$, $J_\mu(u)$ is the Bessel function of order μ , and

$$F = \left[\frac{1}{2} - \frac{1}{2} \text{sgn}(\eta) + \eta \right] (1 - \eta)^{-1}. \quad (52)$$

Thus, the requirement of regularity for all modes is in contradiction with the requirement of completeness for these modes. The problem is to find a condition allowing for irregular at $r \rightarrow 0$ behaviour of the mode with $n = n_c$, i.e. to fix ν_E in Eq.(51). To solve this problem, first of all one has to recall the result of Ref. [27], stating that for the partial Dirac hamiltonian to be essentially self-adjoint, it is necessary and sufficient that a non-square-integrable (at $r \rightarrow 0$) solution exist. Since such a solution does not exist in the case of $n = n_c$, the appropriate partial hamiltonian is not essentially self-adjoint. The Weyl-von Neumann theory of self-adjoint operators (see, e.g., Ref. [28]) is to be employed in order to consider a possibility of the self-adjoint extension for this operator. We show in Appendix B that the self-adjoint extension exists indeed, and the partial hamiltonian at $n = n_c$ is defined on the domain of functions obeying the condition

$$\frac{\lim_{r \rightarrow 0} (rMv/\hbar)^F f_{n_c,s}(r)}{\lim_{r \rightarrow 0} (rMv/\hbar)^{1-F} g_{n_c,s}(r)} = -2^{2F-1} \frac{\Gamma(F)}{\Gamma(1-F)} \tan\left(\frac{\Theta}{2} + \frac{\pi}{4}\right), \quad (53)$$

where $\Gamma(u)$ is the Euler gamma function, M is the parameter of the dimension of mass, and Θ is the self-adjoint extension parameter. Substituting the asymptotics of Eq.(51) at $r \rightarrow 0$ (see, e.g., Ref. [29]) into Eq.(53), one gets the relation fixing parameter ν_E ,

$$\tan(\nu_E) = \text{sgn}(E) \left(\frac{\hbar k}{Mv} \right)^{2F-1} \tan\left(\frac{\Theta}{2} + \frac{\pi}{4}\right). \quad (54)$$

Using the complete set of solutions, it is straightforward to determine the kernel of the resolvent, $\langle r, \varphi | (H - \omega)^{-1} | r', \varphi' \rangle$ (where ω is a complex parameter with dimension of energy), calculate its functional trace, see, e.g., Ref. [19], and find density of states (34). Only the irregular mode contributes to the odd in energy piece of the density of states, which is given by expression

$$\tau(E) =$$

$$= \frac{2(2F-1)\sin(F\pi) \left[\left(\frac{|E|}{Mv^2}\right)^{2F-1} \tan\left(\frac{\Theta}{2} + \frac{\pi}{4}\right) + \left(\frac{|E|}{Mv^2}\right)^{1-2F} \cot\left(\frac{\Theta}{2} + \frac{\pi}{4}\right) \right]}{\pi E \left[\left(\frac{|E|}{Mv^2}\right)^{2(2F-1)} \tan^2\left(\frac{\Theta}{2} + \frac{\pi}{4}\right) - 2\cos(2F\pi) + \left(\frac{|E|}{Mv^2}\right)^{2(1-2F)} \cot^2\left(\frac{\Theta}{2} + \frac{\pi}{4}\right) \right]}. \quad (55)$$

Inserting Eq.(55) into Eq.(36), we calculate the ground state charge,

$$Q = e \operatorname{sgn}_0[(1-2F)\cos\Theta], \quad (56)$$

where

$$\operatorname{sgn}_0(u) = \begin{cases} \operatorname{sgn}(u), & u \neq 0 \\ 0, & u = 0 \end{cases}.$$

The charge, if any, is accumulated in the vicinity of the defect, and its density is given by expression, see Ref. [17],

$$\rho(r) = e \frac{2\sin(F\pi)}{\pi^3(1-\eta)r^2} \int_0^\infty \frac{dw w [K_{1-F}(w) - K_F(w)]}{\left(\frac{\hbar w}{rMv}\right)^{2F-1} \tan\left(\frac{\Theta}{2} + \frac{\pi}{4}\right) + \left(\frac{\hbar w}{rMv}\right)^{1-2F} \cot\left(\frac{\Theta}{2} + \frac{\pi}{4}\right)}, \quad (57)$$

decreasing as an inverse power at large distances from the defect; here $K_\mu(u)$ is the Macdonald function of order μ .

In the case of $\eta < -\frac{1}{2}$ ($N_d = -4, -5, \dots$) there are two or more irregular modes, unless $\eta = -1$ ($N_d = -6$). The case of more than one irregular modes will be considered elsewhere, while in the case of $\eta = -1$ the irregular mode appears at $n = n_c$ with $n_c = -2s$ and has the form

$$\begin{pmatrix} f_{n_c,s}(r) \\ g_{n_c,s}(r) \end{pmatrix} = \frac{1}{2\sqrt{\pi(1-\eta)}} \begin{pmatrix} \sin(\nu_E)J_{-\frac{1}{2}}(kr) + \cos(\nu_E)J_{\frac{1}{2}}(kr) \\ \operatorname{sgn}(E) \left[\sin(\nu_E)J_{\frac{1}{2}}(kr) - \cos(\nu_E)J_{-\frac{1}{2}}(kr) \right] \end{pmatrix}; \quad (58)$$

hence this case corresponds to $F = \frac{1}{2}$ in Eq.(51), yielding the vanishing ground state charge. Our results are summarized in the Table.

If the sign in the exponential function in condition (30) is changed to the opposite, then this corresponds to change $F \rightarrow 1-F$. Our results remain unchanged, if, in addition, shift $\Theta \rightarrow \Theta + \pi$ is performed.

5 Discussion

In the present paper we study the electronic properties of the carbon monolayer (graphene) with disclinations, i.e. $6 - N_d$ -gonal ($N_d \neq 0$) defects inserted in the otherwise perfect twodimensional hexagonal lattice. The effects of the variation of the bond length or the mixing of π - with σ -orbitals caused by curvature of the

lattice surface are neglected, and our consideration, focusing on global aspects of coordination of carbon atoms, is based on the long-wavelength continuum model originating in the tight-binding approximation for the nearest neighbour interactions. Our general conclusion is that the dependence of the electronic properties on the value of N_d is not monotonic, but rather abruptly discontinuous. For some values of N_d the density of states is predicted unambiguously by the theory, whereas, otherwise, its theoretical prediction involves some parameters which should be determined from the experiment.

As it was already noted [20], a defect with odd N_d entwines two sublattices, as well as two inequivalent Fermi points, and in the present paper we show that the correct condition for the electronic wave function involves operator R commuting with the hamiltonian, see Eqs.(30) and (18). However, much stronger impact on electronic properties might be drawn by the fact that for certain N_d irregular modes emerge among the eigenmodes of the hamiltonian. It is instructive to compare two cases when the density of states remains almost the same as for planar graphene, but for different reasons. In the case of the three-pentagon defect ($N_d = 3$), there is entwinement of sublattices and there is no irregular modes; the density of states is calculated (see Appendix A) and shown to coincide exactly with that of planar graphene. In the case of the two-pentagon defect ($N_d = 2$), there is no entwinement and there is an irregular mode; the density of states is even in energy (owing to $F = \frac{1}{2}$, the odd piece vanishes, see Eq.(55)) and almost coincides with that of planar graphene. Thus, we disprove the controversial assertions that the density of states at the Fermi level is nonzero either at $N_d = 2$ [20] or at $N_d = 3$ [21].

The same unambiguous predictions are obtained for a graphene sheet with the two-heptagon defect ($N_d = -2$) and a graphene sheet with a dodecagon or six heptagons ($N_d = -6$): the density of states almost coincides with that of planar graphene. Evidently, the ground state charge is zero in all above cases.

Let us turn now to the cases when our predictions are not unambiguous, since they involve self-adjoint extension parameter Θ . These cases include graphene sheets with following defects: one pentagon ($N_d = 1$), one heptagon ($N_d = -1$), and three heptagons ($N_d = -3$). Contrary to the assertions in Refs.[20, 21], the density of states at the Fermi level is characterized by a divergent, rather than the cusp, behaviour in these cases, see Eq.(55):

$$\tau(E) \underset{E \rightarrow 0}{=} \begin{cases} -\frac{6}{5\pi} \frac{\text{sgn}(E)}{Mv^2} \left(\frac{Mv^2}{|E|}\right)^{\frac{2}{5}} \cot\left(\frac{\Theta}{2} + \frac{\pi}{4}\right), & N_d = 1, \\ \frac{6}{7\pi} \frac{\text{sgn}(E)}{Mv^2} \left(\frac{Mv^2}{|E|}\right)^{\frac{4}{7}} \tan\left(\frac{\Theta}{2} + \frac{\pi}{4}\right), & N_d = -1, \\ -\frac{2}{3\pi} \frac{\text{sgn}(E)}{Mv^2} \left(\frac{Mv^2}{|E|}\right)^{\frac{2}{3}} \cot\left(\frac{\Theta}{2} + \frac{\pi}{4}\right), & N_d = -3. \end{cases} \quad (59)$$

Actually, there are three possibilities: $\cos \Theta > 0$, $\cos \Theta < 0$, and $\cos \Theta = 0$. The

question of which of the possibilities is realized has to be answered by experimental measurements. First, the density of states in the vicinity of the Fermi level can be measured directly in scanning tunnel and transmission electron microscopy. Secondly, the ground state charge can be measured also, and our prediction, see Eq.(56) or the Table, is

$$Q|_{N_d=1} = -Q|_{N_d=-1} = Q|_{N_d=-3}, \quad (60)$$

while the ground state charge density decreases by power law at large distances from the defect, see Eq.(57),

$$\rho(r) \underset{r \rightarrow \infty}{=} \begin{cases} e \frac{9 \sin(\pi/5)}{20\pi^2} \frac{\Gamma(\frac{13}{10})\Gamma(\frac{11}{10})}{\Gamma(\frac{4}{5})} \frac{1}{r^2} \left(\frac{\hbar}{rMv}\right)^{\frac{3}{5}} \cot\left(\frac{\Theta}{2} + \frac{\pi}{4}\right), & N_d = 1, \\ -e \frac{9 \sin(2\pi/7)}{35\pi^2} \frac{\Gamma(\frac{17}{14})\Gamma(\frac{13}{14})}{\Gamma(\frac{5}{7})} \frac{1}{r^2} \left(\frac{\hbar}{rMv}\right)^{\frac{3}{7}} \tan\left(\frac{\Theta}{2} + \frac{\pi}{4}\right), & N_d = -1, \\ e \frac{\sqrt{3}}{12\pi^2} \frac{\Gamma(\frac{7}{6})\Gamma(\frac{5}{6})}{\Gamma(\frac{2}{3})} \frac{1}{r^2} \left(\frac{\hbar}{rMv}\right)^{\frac{1}{3}} \cot\left(\frac{\Theta}{2} + \frac{\pi}{4}\right), & N_d = -3. \end{cases} \quad (61)$$

The results for the ground state charge in the case of $\cos \Theta > 0$ agree with the results of numerical atomistic calculation of the bond network with the use of recursion methods [30]. The pentagonal defect, as well as the three-heptagon one, is attractive, and the heptagonal defect is repulsive to electrons. The charge, negative or positive, is accumulated around the defect, and, at large distances from it, the decrease is the strongest one for a pentagon and the weakest one for three heptagons.

It should be noted that at $\cos \Theta \neq 0$ and $F \neq \frac{1}{2}$ scale invariance is broken, and the appearance of parameter M with dimension of mass evinces this. In general, irregular mode (51) diverges at the origin as $r^{-\nu}$ with $\nu < 1$. Scale invariance is respected by the condition of minimal irregularity [31, 14, 15],

$$\Theta = \begin{cases} \frac{\pi}{2}(\text{mod}2\pi), & 0 < F < \frac{1}{2}, \\ -\frac{\pi}{2}(\text{mod}2\pi), & \frac{1}{2} < F < 1, \end{cases} \quad (62)$$

which restricts the behaviour of the irregular mode at the origin to $r^{-\nu}$ with $\nu < \frac{1}{2}$. Thus, both scale invariance and minimal irregularity favour definitely the choice of $\cos \Theta = 0$, when the density of states and the ground state charge are trivial. It would be inspiring, if the experiment could prefer other choices.

Acknowledgements

We would like to thank V.P. Gusynin for stimulating discussions. The research was supported in part by the Swiss National Science Foundation under the SCOPES project No. IB7320-110848. Yu.A.S. acknowledges the support of the

State Foundation for Fundamental Research of Ukraine (grant F16-457-2007) and INTAS (grant No. 05-1000008-7865). N.D.V. acknowledges the INTAS support through the PhD Fellowship Grant for Young Scientists (No. 05-109-5333).

Appendix A

In the case of $\eta = \frac{1}{2}$ hamiltonian H_s (42) takes form

$$H_s = \hbar v \left[i\sigma^2 \partial_r - \sigma^1 r^{-1} \left(2is\partial_\varphi + \frac{3}{2} + \frac{1}{2}\sigma^3 \right) \right]. \quad (\text{A.1})$$

The kernel of the resolvent (the Green's function) of the hamiltonian is presented as

$$\langle r, \varphi | (H_s - \omega)^{-1} | r', \varphi' \rangle = \frac{1}{2\pi} \sum_{n \in \mathbb{Z}} e^{i(n + \frac{s}{2})(\varphi - \varphi')} \begin{pmatrix} a_n^{11}(r, r') & a_n^{21}(r, r') \\ a_n^{12}(r, r') & a_n^{22}(r, r') \end{pmatrix}, \quad (\text{A.2})$$

where the radial components satisfy equations

$$\begin{aligned} & \begin{pmatrix} -\omega & \hbar v(\partial_r + r^{-1}2sn) \\ \hbar v[-\partial_r + r^{-1}(2sn-1)] & -\omega \end{pmatrix} \begin{pmatrix} a_n^{11}(r, r') & a_n^{21}(r, r') \\ a_n^{12}(r, r') & a_n^{22}(r, r') \end{pmatrix} = \\ & = \begin{pmatrix} -\omega & \hbar v(\partial_{r'} + r'^{-1}2sn) \\ \hbar v[-\partial_{r'} + r'^{-1}(2sn-1)] & -\omega \end{pmatrix} \begin{pmatrix} a_n^{11}(r, r') & a_n^{12}(r, r') \\ a_n^{21}(r, r') & a_n^{22}(r, r') \end{pmatrix} = \\ & = \frac{2}{r} \delta(r - r') \begin{pmatrix} 1 & 0 \\ 0 & 1 \end{pmatrix}; \end{aligned} \quad (\text{A.3})$$

note that a factor before the delta-function is due to $(\det g_{jj'})^{-\frac{1}{2}} = [(1 - \eta)r]^{-1}$. The radial components can be found in the form

$$a_n^{kk'} = \int_0^\infty \frac{dp p}{\hbar^2 v^2 p^2 - \omega^2} a_{n,p}^{kk'}(r, r'), \quad (\text{A.4})$$

where

$$\begin{aligned} a_{n,p}^{11}(r, r') &= 2\omega J_{2sn-1}(pr) J_{2sn-1}(pr'), \\ a_{n,p}^{12}(r, r') &= 2\hbar v p J_{2sn}(pr) J_{2sn-1}(pr'), \\ a_{n,p}^{21}(r, r') &= 2\hbar v p J_{2sn-1}(pr) J_{2sn}(pr'), \\ a_{n,p}^{22}(r, r') &= 2\omega J_{2sn}(pr) J_{2sn}(pr'). \end{aligned} \quad (\text{A.5})$$

Putting $\varphi' = \varphi$ and taking trace of matrix (A.2), one gets

$$\begin{aligned} \text{tr}\langle r, \varphi | (H_s - \omega)^{-1} | r', \varphi \rangle &= \frac{1}{2\pi} \sum_{n \in \mathbb{Z}} [a_n^{11}(r, r') + a_n^{22}(r, r')] = \\ &= \frac{\omega}{\pi} \int_0^\infty \frac{dp p}{\hbar^2 v^2 p^2 - \omega^2} \sum_{n \in \mathbb{Z}} [J_{2sn-1}(pr) J_{2sn-1}(pr') + J_{2sn}(pr) J_{2sn}(pr')]. \end{aligned} \quad (\text{A.6})$$

The summation is performed with the use of the Neumann's addition theorem (see, e.g., Ref. [29]), yielding the expression,

$$\text{tr}\langle r, \varphi | (H_s - \omega)^{-1} | r', \varphi \rangle = \frac{\omega}{\pi} \int_0^\infty \frac{dp p}{\hbar^2 v^2 p^2 - \omega^2} J_0[p(r - r')], \quad (\text{A.7})$$

which is badly divergent at $r' \rightarrow r$. To tame the divergence, we define regularized kernel

$$\begin{aligned} \langle r, \varphi | (H_s - \omega)^{-1} \exp(-tH_s^2) | r', \varphi' \rangle &= \frac{1}{2\pi} \int_0^\infty \frac{dp p \exp(-t\hbar^2 v^2 p^2)}{\hbar^2 v^2 p^2 - \omega^2} \times \\ &\times \sum_{n \in \mathbb{Z}} e^{i(n + \frac{s}{2})(\varphi - \varphi')} \begin{pmatrix} a_{n,p}^{11}(r, r') & a_{n,p}^{21}(r, r') \\ a_{n,p}^{12}(r, r') & a_{n,p}^{22}(r, r') \end{pmatrix}, \end{aligned} \quad (\text{A.8})$$

where $t > 0$ is the regularization parameter. Now the limit $r' \rightarrow r$ can be taken safely, yielding

$$\begin{aligned} \text{tr}\langle r, \varphi | (H_s - \omega)^{-1} \exp(-tH_s^2) | r, \varphi \rangle &= \frac{\omega}{\pi} \int_0^\infty \frac{dp p \exp(-t\hbar^2 v^2 p^2)}{\hbar^2 v^2 p^2 - \omega^2} = \\ &= \frac{\omega}{2\pi \hbar^2 v^2} E_1(-t\omega^2), \end{aligned} \quad (\text{A.9})$$

where

$$E_1(u) = \int_u^\infty \frac{du}{u} e^{-u}$$

is the exponential integral (see Ref. [29]). Note that, actually, we have reiterated the derivation for the case of the planar graphene sheet ($\eta = 0$): the only difference is that in the latter case all factors of 2 (including those at the order of Bessel functions) in the right hand sides of Eq.(A.5) are absent.

Since Eq.(A.9) is independent of r and φ , the integration over the surface yields a factor of its area:

$$\text{Tr}(H_s - \omega)^{-1} \exp(-tH_s^2) = \frac{S\omega}{2\pi\hbar^2 v^2} E_1(-t\omega^2). \quad (\text{A.10})$$

The divergence of the last quantity in the limit $t \rightarrow 0_+$ does not contribute to the density of states, Eq.(34). This is due to a specific form of a discontinuity of the exponential integral at negative real values of its argument, $\text{Im } E_1(-u \mp i0) = \pm i\pi$ ($u > 0$). Consequently, we get finite result (35).

Appendix B

The partial hamiltonian corresponding to $n = n_c$ takes form, see Eqs.(45)-(47) and (52),

$$h = \hbar v \begin{pmatrix} 0 & \partial_r + r^{-1}(1 - F) \\ -\partial_r - r^{-1}F & 0 \end{pmatrix}. \quad (\text{B.1})$$

Let h be defined on the domain of functions $\xi^0(r)$ that are regular at $r = 0$. Then its adjoint h^\dagger which is defined by relation

$$\int_0^\infty dr r(1 - \eta)[h^\dagger \xi(r)]^\dagger \xi^0(r) = \int_0^\infty dr r(1 - \eta)[\xi(r)]^\dagger h \xi^0(r) \quad (\text{B.2})$$

acts on the domain of functions $\xi(r)$ that are not necessarily regular at $r = 0$. So the question is whether the domain of definition of h can be extended, resulting in both the operator and its adjoint being defined on the same domain of functions. To answer this, one has to construct the eigenspaces of h^\dagger with complex eigenvalues. They are spanned by the linearly independent square-integrable solutions corresponding to the pair of purely imaginary eigenvalues,

$$h^\dagger \xi^\pm(r) = \pm i M v^2 \xi^\pm(r), \quad (\text{B.3})$$

where $M v^2$ is inserted for the dimension reasons. It is straightforward to show that only one pair of such solutions exists

$$\xi^\pm(r) = \frac{1}{N} \begin{pmatrix} e^{\pm i \frac{\pi}{4}} K_F(r M v / \hbar) \\ e^{\mp i \frac{\pi}{4}} K_{1-F}(r M v / \hbar) \end{pmatrix}, \quad (\text{B.4})$$

where N is a certain normalization factor. Thus, the deficiency index is equal to (1,1), and, according to the Weyl-von Neumann theory of self-adjoint operators

(see Ref. [28]), the self-adjoint extension of operator h is defined on the domain of functions of the form

$$\begin{pmatrix} f_{n_c,s}(r) \\ g_{n_c,s}(r) \end{pmatrix} = \xi^0(r) + c [\xi^+(r) - e^{-i\Theta}\xi^-(r)], \quad (\text{B.5})$$

where c is a complex constant and Θ is a real continuous parameter. Using the asymptotics of the Macdonald function at small values of its argument (see Ref. [29]), we get

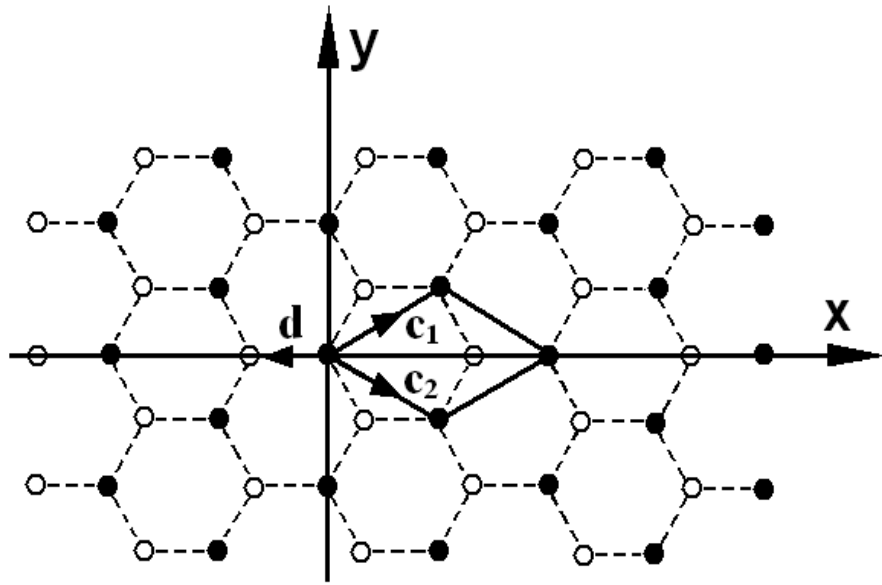
$$\begin{pmatrix} f_{n_c,s}(r) \\ g_{n_c,s}(r) \end{pmatrix} \underset{r \rightarrow 0}{=} \frac{2c e^{-i\frac{\Theta}{2}}}{iN} \begin{pmatrix} -\sin\left(\frac{\Theta}{2} + \frac{\pi}{4}\right) 2^F \Gamma(F) (rMv/\hbar)^{-F} \\ \cos\left(\frac{\Theta}{2} + \frac{\pi}{4}\right) 2^{1-F} \Gamma(1-F) (rMv/\hbar)^{-1+F} \end{pmatrix}, \quad (\text{B.6})$$

which can be rewritten in the form of Eq.(53).

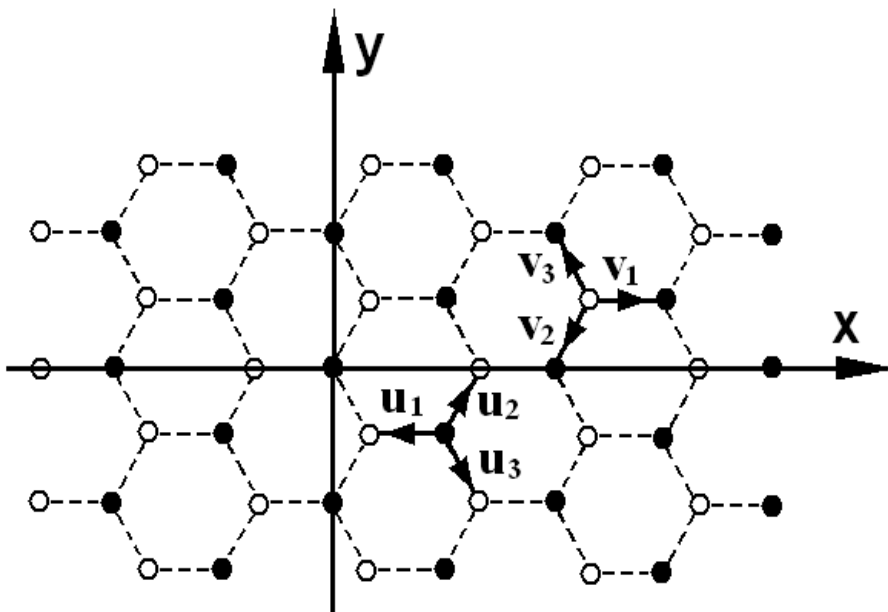
References

- [1] K.S. Novoselov, D. Jiang, F. Schedin, T.J. Booth, V.V. Khotkevich, S.V. Morozov, and A.K. Geim, Proc. Nat. Acad. Sci. USA 102 (2005) 10451.
- [2] A.K. Geim and K.S. Novoselov, Nature Mater. 6 (2007) 183.
- [3] K.S. Novoselov, A.K. Geim, S.V. Morozov, D. Jiang, M.I. Katsnelson, I.V. Grigorieva, S.V. Dubonos, and A.A. Firsov, Nature 438 (2005) 197.
- [4] Y. Zhang, Y.-W. Tan, H.L. Stormer, and P. Kim, Nature 438 (2005) 201.
- [5] A.C. Neto, F. Guinea, and N.M. Peres, Physics World 19 No.11 (2006) 33.
- [6] D.P. DiVincenzo and E.J. Mele, Phys. Rev. B 29 (1984) 1685.
- [7] G.W. Semenoff, Phys. Rev. Lett. 53 (1984) 2449.
- [8] R. Jackiw and C. Rebbi, Phys. Rev. D 13 (1976) 3398.
- [9] A.A. Abrikosov, Sov. Phys. JETP 5 (1957) 1174.
- [10] H.B. Nielsen and P. Olesen, Nucl. Phys. B 61 (1973) 45.
- [11] R. Jackiw and P. Rossi, Nucl. Phys. B 190 (1981) 681.
- [12] C.-Y. Hou, C. Chamon, and C. Mudry, Phys. Rev. Lett. 98 (2007) 186809.
- [13] R. Jackiw and S.-Y. Pi, Chiral gauge theory for graphene, cond-mat/0701760; Phys. Rev. Lett., May 2007 (to be published).

- [14] Yu.A. Sitenko, Phys. Lett. B 387 (1996) 334.
- [15] Yu.A. Sitenko, Phys. Atom. Nucl. 60 (1997) 2102; (E) 62 (1999) 1084.
- [16] Yu.A. Sitenko, Mod. Phys. Lett. A 14 (1999) 701; Phys. Rev. D 60 (1999) 125017.
- [17] Yu.A. Sitenko, Ann. Phys. 282 (2000) 167.
- [18] P. de Sousa Gerbert and R. Jackiw, Commun. Math. Phys. 124 (1989) 229.
- [19] Yu.A. Sitenko and V.M. Gorkavenko, Nucl. Phys. B 679 (2004) 597.
- [20] P.E. Lammert and V.H. Crespi, Phys. Rev. Lett. 85 (2000) 5190.
- [21] V.A. Osipov, E.A. Kochetov, and M. Pudlak, JETP 96 (2003) 140; R. Pincak and V.A. Osipov, Phys. Lett. A 314 (2003) 315.
- [22] A. Cortijo and M.A.H. Vozmediano, Nucl. Phys. B 763 (2007) 293.
- [23] J. Gonzalez, F. Guinea, and M.A.H. Vozmediano, Nucl. Phys. B 406 (1993) 771.
- [24] A. Krishnan, E. Dujardin, M.M.J. Treacy, J. Hugdahl, S. Lynum, and T.W. Ebbesen, Nature 388 (1997) 451.
- [25] S. Ihara, S. Itoh, K. Akagi, R. Tamura, and M. Tsukada, Phys. Rev. B 54 (1996) 14713.
- [26] N.D. Birrel and P.C.W. Davies, Quantum Fields in Curved Space (Cambridge Univ. Press, Cambridge, 1982).
- [27] J. Weidmann, Math. Z. 119 (1971) 349.
- [28] S. Albeverio, F. Gesztezy, R. Hoegh-Krohn, and H. Holden, Solvable Models in Quantum Mechanics (Springer-Verlag, Berlin, 1988).
- [29] Handbook of Mathematical Functions, edited by M. Abramowitz and I.A. Stegun (Dover, New York, 1972).
- [30] R. Tamura and M. Tsukada, Phys. Rev. B 49 (1994) 7697; R. Tamura, K. Akagi, M. Tsukada, S. Itoh, and S. Ihara, Phys. Rev. B 56 (1997) 1404.
- [31] Yu.A. Sitenko, Nucl. Phys. B 342 (1990) 655; Phys. Lett. B 253 (1991) 138.



a)



b)

Figure 1: The planar honeycomb lattice as a composition of two triangular sublattices. The primitive cell with basis vectors \mathbf{c}_1 and \mathbf{c}_2 is depicted in a), the triads \mathbf{u}_j and \mathbf{v}_j connecting different sublattices are depicted in b).

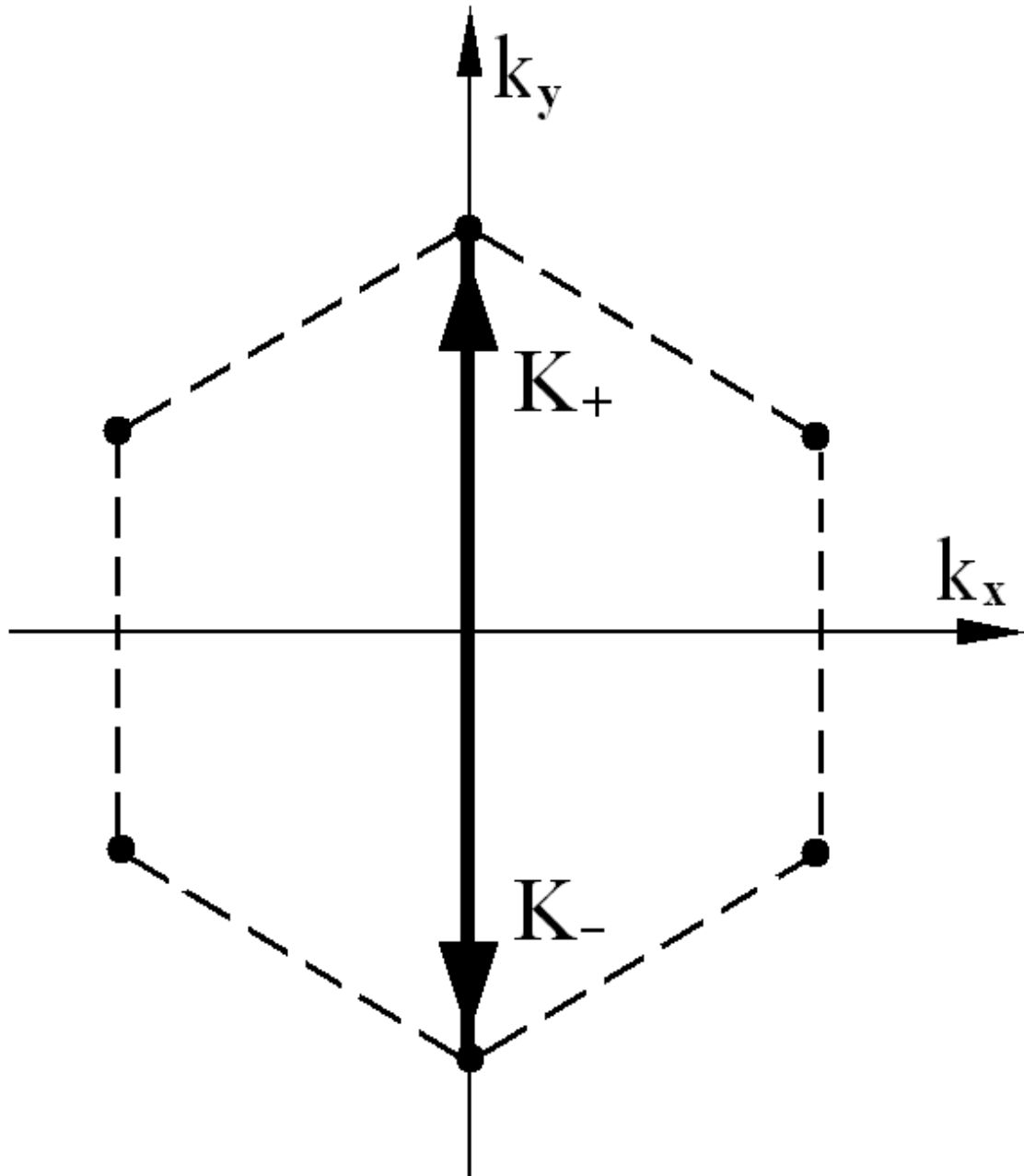
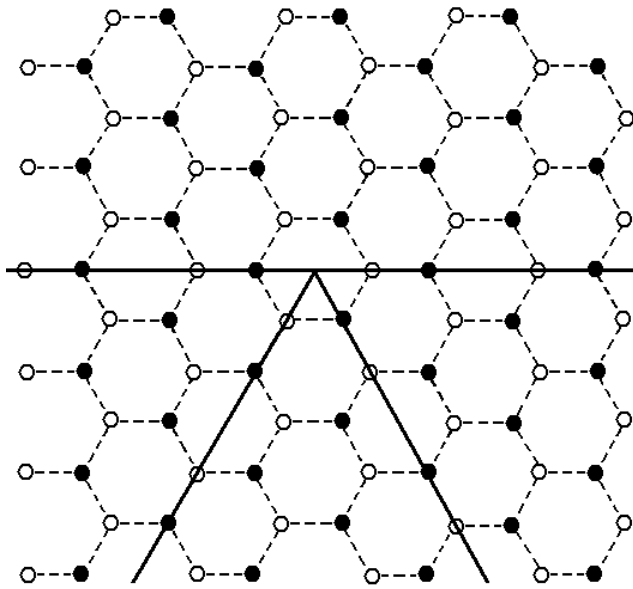
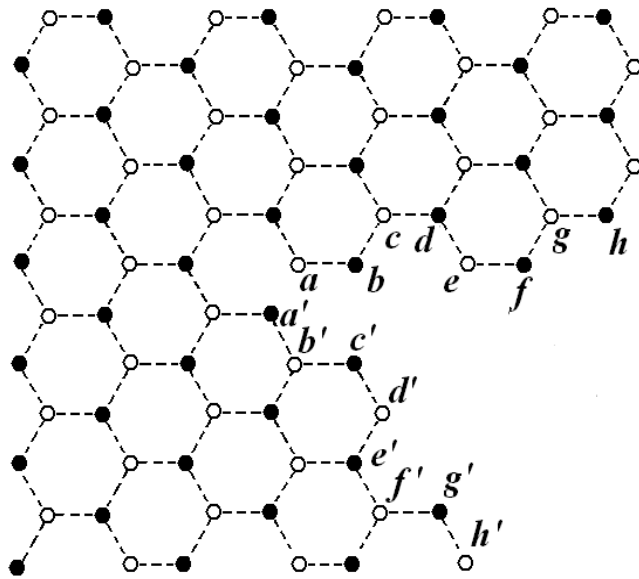


Figure 2: The first Brillouin zone is a hexagon with opposite sides identified, and, therefore, next to neighbouring corners are equivalent; two inequivalent ones can be chosen as lying on a vertical line.



a)



b)

Figure 3: Formation of a topological defect in graphene: a) one, two, or three sectors of 60° are removed from the lattice, b) if one sector is removed, then sites of different sublattices are identified, a and a' , b and b' , c and c' , etc.

Table:

The ground state charge in the case of the existence of the one irregular mode in the set of eigenmodes of the hamiltonian

N_d	2	1	-1	-2	-3	-6
F	1/2	1/5	5/7	1/2	1/3	1/2
Q	0	$e \operatorname{sgn} n_0 (\cos \Theta)$	$-e \operatorname{sgn} n_0 (\cos \Theta)$	0	$e \operatorname{sgn} n_0 (\cos \Theta)$	0